



CHORUS

This is the accepted manuscript made available via CHORUS. The article has been published as:

Reynolds number scaling of the influence of boundary layers on the global behavior of laboratory quasi-Keplerian flows

E. M. Edlund and H. Ji

Phys. Rev. E **92**, 043005 — Published 6 October 2015

DOI: [10.1103/PhysRevE.92.043005](https://doi.org/10.1103/PhysRevE.92.043005)

Reynolds number scaling of the influence of boundary layers on the global behavior of laboratory quasi-Keplerian flows

E. M. Edlund and H. Ji

Princeton Plasma Physics Laboratory,

Princeton, New Jersey 08543, USA

Abstract

We present fluid velocity measurements in a modified Taylor-Couette device operated in the quasi-Keplerian regime where it is observed that nearly-ideal flows exhibit self-similarity under scaling of the Reynolds number. In contrast, non-ideal flows show progressive departure from ideal Couette as the Reynolds number is increased. We present a model that describes the observed departures from ideal Couette rotation as a function of the fluxes of angular momentum across the boundaries, capturing the dependence on Reynolds number and boundary conditions.

I. INTRODUCTION

That the global properties of an extended system may be mapped to the boundaries is an idea that has found success in holographic theories of general relativistic systems [1, 2], and in magnetically confined plasmas [3, 4]. We report on a similar behavior observed in incompressible hydrodynamic flows in a Taylor-Couette apparatus where it is observed that certain characteristics of the global flow are largely dictated by the boundaries. This finding is particularly relevant for experiments that examine quasi-Keplerian (QK) flows, that is, rotation satisfying $0 < q < 2$ where $q = -d \ln \Omega / d \ln r$, Ω is the fluid angular velocity and r is the radial coordinate, as models of astrophysical systems, namely accretion disks. Numerous recent studies have commented on the hydrodynamic stability of such systems [5–8], with extensions to magnetohydrodynamics in electrically conducting fluids [9–13].

While there is some disagreement between studies as to whether hydrodynamic turbulence can be induced in QK flows, the balance seems to lean toward the negative, at least insofar as incompressible turbulence is considered, and points to the important role of magnetohydrodynamic effects in astrophysical systems. However, while it is known that QK flows are linearly stable it remains unknown whether there exists a nonlinear transition to turbulence, even for incompressible hydrodynamic systems. Some experiments [5–7] and simulations [14] indicate that such a transition is not likely, while others present evidence that suggests that a subcritical transition may exist [8] and some simulations find significant transient growth of perturbations that may allow for nonlinear effects to enter [15]. Fluid experiments in other regimes of operation that are not astrophysically-relevant have observed bi-stability [16, 17], suggesting that should a similar mechanism exist for QK systems then a subcritical pathway to turbulence may explain angular momentum transport in accretion disks [18]. We show in this work that the influence of the boundaries is intimately connected to the global structure of flows in Taylor-Couette experiments and, by extension, is also related to the tendency of these systems to generate and sustain turbulence.

One of the long-standing challenges of Taylor-Couette experiments in the quest to understand angular momentum transport in astrophysically-relevant flows has been the parasitic presence of Ekman circulation (secondary circulation) induced by the mismatch between the fluid velocity and the solid body rotation of the axial boundaries. A significant reduction in Ekman circulation has been realized in experiment by using axial boundaries that are

split into multiple rings capable of differential rotation. Under particular boundary conditions, azimuthal velocity profiles of the fluid can be generated that very nearly match that of ideal Couette rotation [5, 7, 19, 20], the rotation profile that is expected in the absence of axial influences for a constant radial flux of angular momentum. In contrast, studies in the “classical” configuration where the axial boundaries rotate with the outer cylinder have shown performance that further deviates from ideal Couette as the Reynolds number is increased [21]. Such trends are revealing of whether these systems are dominated by boundary interactions or internal dynamics, a distinction with important consequences for the applicability of such experiments to interpretation of astrophysical systems, especially at large Reynolds numbers. First, through the experiments reported here we identify two necessary criteria that define constraints on the boundary configurations that allow near-ideal flows to develop. We then discuss the competing roles of radial (Stewartson) boundary layers and axial (Ekman) boundary layers, from which we develop a model that describes the quantitative departure of the rotation profiles from ideal Couette flow as a function of the angular momentum fluxes through the boundaries.

II. EXPERIMENTAL APPARATUS

A Taylor-Couette (TC) device is a system of coaxial cylinders that rotate independently of each other with the experimental fluid region between. The TC apparatus used in these studies, called the Hydrodynamic Turbulence Experiment (HTX), is a modified version of the classical device in that the axial boundaries in HTX are segmented to allow differential rotation across the boundaries [7]. The inner cylinder radius is $r_1 = 6.9$ cm and the outer cylinder radius is $r_2 = 20.3$ cm. The inner radius and outer radius of the independent rings are defined by the parameters r_3 and r_4 , respectively. The axial length of the experimental volume is $L = 39.8$ cm, giving an aspect ratio of $\Gamma = L/(r_2 - r_1) = 2.97$ (see Fig. 1). Corresponding components on the top and bottom are driven by the same motor so that the system is up-down symmetric. The angular velocities of the inner cylinder, outer cylinder and rings are identified by Ω_1 , Ω_2 and Ω_3 , respectively. Rotary encoders report the speed of the motors to the control system.

A laser Doppler velocimeter (LDV) diagnostic system is used to measure the local, azimuthal velocity (v_θ), which in the experiments reported here were measured at the midplane

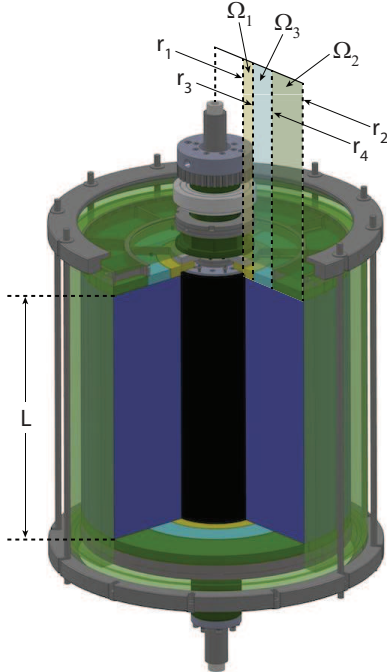


FIG. 1. (color online) Illustration of the HTX device at PPPL showing the segmented axial boundaries (yellow, blue and green segments), the inner cylinder in black, the outer cylinder in green and the working fluid in dark blue.

of the device. The LDV system is calibrated by measuring fluid flow in solid body for which, after spin-up, the only velocity component is v_θ , which is a unique function of the motor speeds. For these studies we define the global shear Reynolds number as $Re_s = r_g^2 \Delta\Omega / \nu$, where $r_g = (r_1 r_2)^{1/2}$ is the geometric-mean radius, $\Delta\Omega = \Omega_1 - \Omega_2$ and ν is the kinematic viscosity, approximately $1 \times 10^{-6} \text{ m}^2/\text{s}$ for water.

III. OBSERVATIONS

The core observation of this work is summarized in Fig. 2, presenting flows under two different values of normalized shear ($q = 1.8$ and $q = 1.5$) and three different boundary conditions: **Split**, **Optimized**, and **Ekman**. For the $q = 1.8$ cases these configuration speeds, reported as Ω_1 - Ω_3 - Ω_2 , are multiples of 350-350-50 RPM (**Split**), 350-185-50 RPM (**Optimized**), and 350-50-50 RPM (**Ekman**). For the $q = 1.5$ these are 250-250-50 RPM (**Split**), 250-140-50 RPM (**Optimized**), and 250-50-50 RPM (**Ekman**). The reference profile for these studies is described by ideal Couette rotation, defined in terms of angular velocity

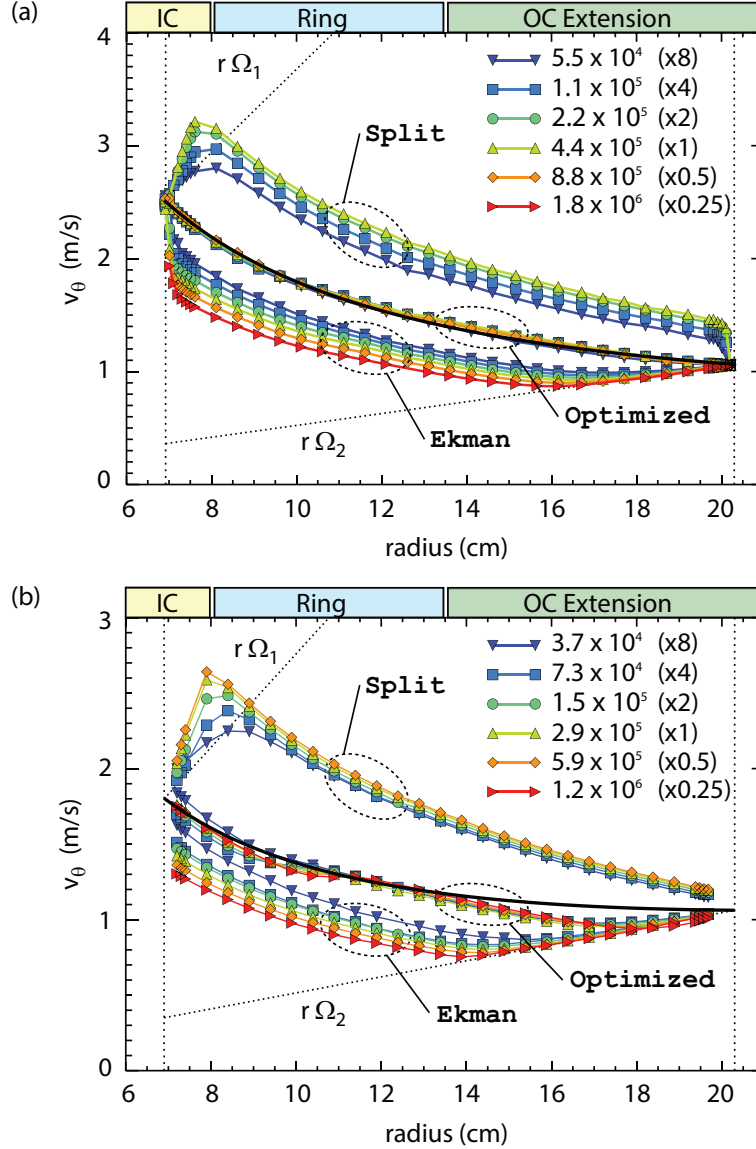


FIG. 2. (color online) Scaled measurements of v_θ at various Re_s for (a) $q = 1.8$ and (b) $q = 1.5$.

as $\Omega_C(r) = \Omega_A + \Omega_B(r_g/r)^2$, where $\Omega_A = (r_2^2\Omega_2 - r_1^2\Omega_1)/(r_2^2 - r_1^2)$, $\Omega_B = r_g^2(\Omega_1 - \Omega_2)/(r_2^2 - r_1^2)$. As a function of azimuthal velocity the Couette solution is $v_C(r) = r\Omega_C$. It is interesting that while the **Ekman** and **Split** configurations exhibit progressive departure from ideal Couette as the Reynolds number is increased, the shape of the **Optimized** cases is nearly invariant with respect to scaling of the Reynolds number.

A. Necessary conditions for near-ideal flows

Recognizing that the axial boundaries in the `Split` cases will tend to increase the angular momentum flux to the bulk, and conversely for the `Ekman` cases, we begin by considering the ansatz that the balance of angular momentum fluxes across the axial boundaries determines the deviation from ideal Couette. A continuous variation of Ω_3 from Ω_2 to Ω_1 would then suggest that there is some intermediate state for which the profile must pass close to ideal Couette rotation. We now address whether there is a method for predicting this optimal value of Ω_3 .

The transition between the bulk flow and the walls of the TC device, which may move at very different speeds, occurs over thin boundary layers. The structure of these boundary layers depends on whether we are considering the balance of forces in the axial or radial directions. The bulk flow transitions to the axial boundary speeds over Ekman boundary layers whose thickness scales like $\delta_E \sim r\text{Re}_b^{-1/2}$, and in the ideal model of radial boundaries, over Stewartson boundary layers that scale like $\delta_S \sim r\text{Re}_b^{-1/4}$, where $\text{Re}_b = r^2\Omega_b/\nu$ is a local Reynolds number particular to the boundary location r with boundary speed Ω_b [22–24]. The fluxes of angular momentum across these boundary layers, being inversely proportional to the boundary layer thickness, do not scale proportionally, and hence we anticipate that self-similarity of the global properties need not be preserved as the Reynolds number is scaled. Thus, while the observed variation in the shape of the `Ekman` and `Split` profiles is expected, it comes as some surprise that the `Optimized` profiles are effectively independent of the Reynolds number.

The experiments reported here showed no significant temporal variation in the mean values, hence, it can be stated that in steady-state the net flux of angular momentum into these flows must sum to zero, that is, $\Phi_1 + \Phi_2 + 2\Phi_z = 0$ where Φ_1 and Φ_2 are the fluxes integrated over the inner and outer cylinders, respectively, and Φ_z is the axial flux integrated over each axial boundary (with inward towards the fluid defined as a positive flux). The ideal Couette profile is the response to a constant radial flux of angular momentum, implying that $\Phi_2 = -\Phi_1$ and that the axial fluxes of angular momentum are everywhere zero. Such a state can be imagined in a TC system with free-slip conditions on the axial boundaries, or with a continuously variable boundary that can perfectly match the ideal Couette profile, conditions that will result in vanishing stress at the axial boundaries. The radial flux of

angular momentum under these conditions (which we call Φ_C , the Couette flux) has a magnitude equal to

$$\Phi_C = \Phi_0 \frac{r_g^2}{r_2^2 - r_1^2} \text{Re}_s, \quad (1)$$

where $\Phi_0 = 4\pi\rho\nu^2L$. As an aside, it is interesting to note that $\Phi_C = \Phi_0 \text{Re}_s$ when the radius ratio (r_2/r_1) is equal to the golden ratio.

Even though there is, in general, a large mismatch between fluid and axial boundary speeds, we find that the flows under the `Optimized` boundary conditions very closely approximate the ideal Couette profile, and therefore have a nearly constant radial flux of angular momentum. We now show that rather than satisfying the condition that the axial flux of angular momentum everywhere vanishes, these flows satisfy a much weaker constraint: it is the surface integral of the axial angular momentum flux that vanishes, that is, $\Phi_z \approx 0$.

To calculate the axial flux of angular momentum, being proportional to $d\Omega/dz$, we make the assumption that $d\Omega/dz \approx \Delta\Omega_E/\delta_E$, where $\Delta\Omega_E = \Omega_b - \Omega_{fl}$ is the difference of the boundary angular velocity (Ω_b) and the fluid angular velocity just inside the Ekman boundary layer (Ω_{fl}), and that $\delta_E = \alpha_E (\nu/\Omega_b)^{1/2}$ represents the thickness of an Ekman boundary layer with an unknown numerical constant α_E . Defining the normalized quantities $\omega = \Omega/\Delta\Omega$ (recalling, $\Delta\Omega = \Omega_1 - \Omega_2$), $\omega_b = \Omega_b/\Delta\Omega$, $s_1 = r_1/r_g$ and $s_2 = r_2/r_g$, we have

$$\Phi_z = \Phi_0 \frac{r_g}{2\alpha_E L} \text{Re}_s^{3/2} \int_{s_1}^{s_2} (\omega_b - \omega) \omega_b^{1/2} s^3 ds. \quad (2)$$

That the radial flux of angular momentum under ideal Couette rotation (Eq. 1) scales like Re_s , whereas Φ_z scales like $\text{Re}_s^{3/2}$ means that unless steps are taken to force the integral in Eq. 2 to zero, there will always exist a Reynolds number beyond which the axial flux will overwhelm the Couette flux and cause the flow to depart from ideal rotation, regardless of aspect ratio. From Eq. 2 we can immediately conclude that TC devices of the ‘‘classical’’ geometry with the axial boundaries co-rotating with either the inner cylinder or outer cylinder will always have non-zero Φ_z and can therefore never be a good model for astrophysical systems at sufficiently high Reynolds numbers to be of interest. In looking for the conditions under which ideal Couette flow may be generated, we set $\omega = \omega_C$ and search for the boundary conditions (the ω_b) that cause the integral of Eq. 2 to vanish.

Figure 3 summarizes fluid velocity measurements over a scan of Ω_3 for $q = 1.8$ flows for

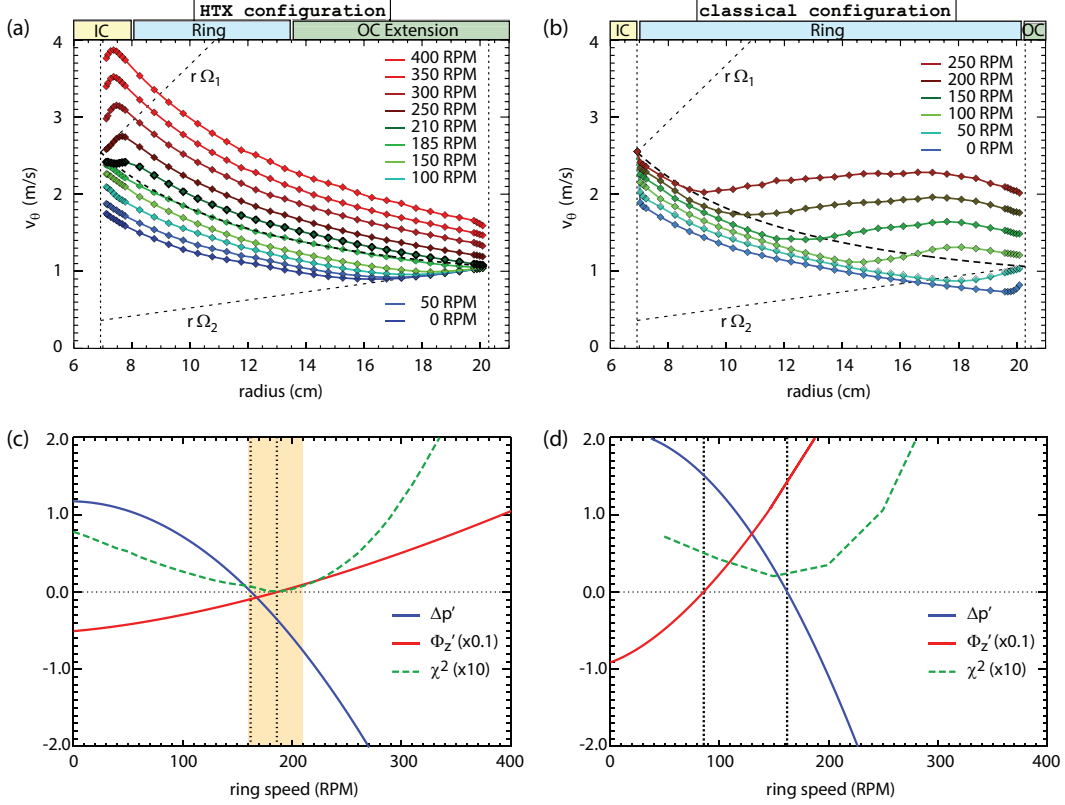


FIG. 3. (color online) Experiments conducted in $q = 1.8$ flows showing v_θ as a function of Ω_3 for the (a) HTX and (b) **wide-ring** geometries, progressing from low ring speeds (bottom curves) to higher ring speeds (upper curves). In panels (c) and (d) the experimental χ^2 (dashed green), for the measured profiles relative to the ideal Couette profile for these boundary conditions, is plotted against the calculated axial flux of angular momentum from Eq. 2 (red, increasing function) and the pressure differential from Eq. 3 (blue, decreasing function) for the HTX and **wide-ring** geometries, respectively. Φ_z is normalized by Φ_C and Δp is normalized by the kinetic energy density for ideal Couette flow. The vertical dotted lines indicate the zeros of Δp and Φ_z .

two axial boundary configurations: the HTX configuration with $r_3 = 7.8$ cm and $r_4 = 13.5$ cm, and a **wide-ring** configuration with rings that span the entire radial gap. These experiments show that the HTX configuration produces an exceptional match to the ideal Couette profile for a narrow range of ring speeds centered about 185 RPM, with very low fluctuation levels spanning the entire gap [7]. Importantly, the boundary conditions that generate near-ideal flows for the HTX configuration include the zero crossing of Φ_z (panel c). However, the **wide-ring** case also has a zero in Φ_z , near 85 RPM (panel d), yet its flows never resemble

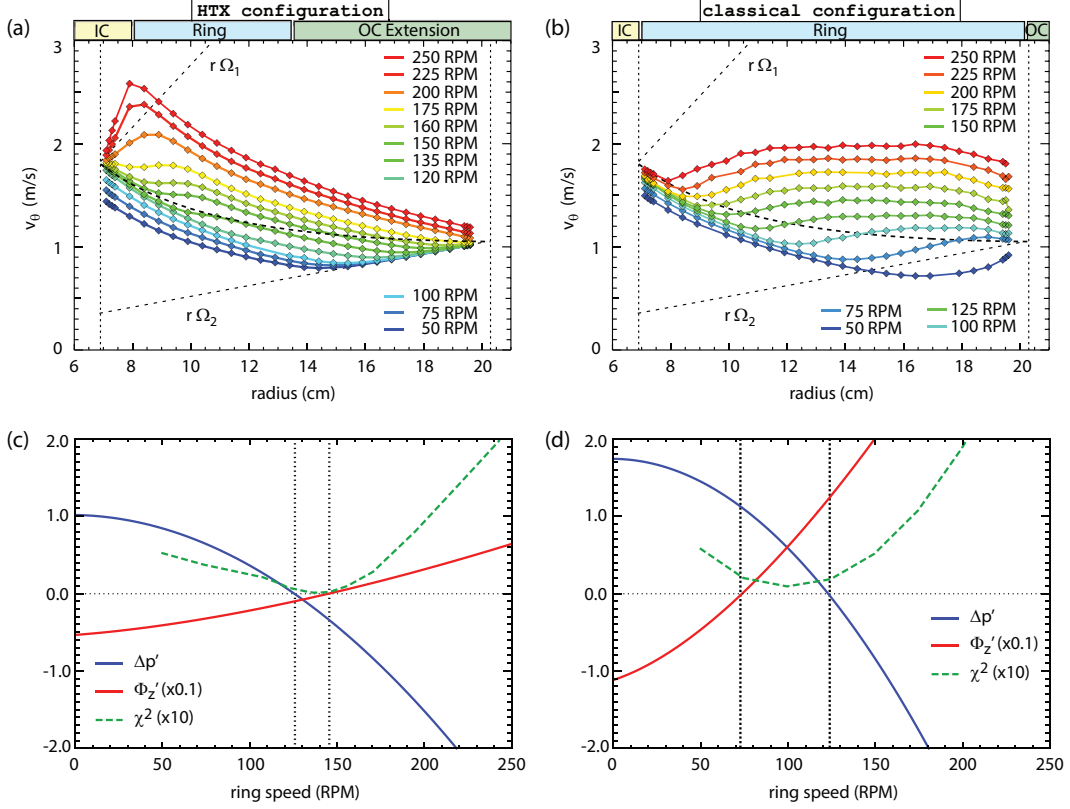


FIG. 4. (color online) Same as Fig. 3 except for $q = 1.5$.

ideal Couette, indicating that the vanishing of Φ_z is a necessary but not sufficient condition for achieving near-ideal flows.

The role of the axial boundaries in dictating global performance has also been interpreted through the competition of pressures from the bulk flow and from the boundary flow that is viscously coupled to the axial boundaries [25, 26]. The tendency to drive secondary flows was shown to be consistent with whether the bulk pressure is larger than (Ekman circulation) or smaller than (anti-Ekman circulation) the boundary pressure. Following the intuition motivated by these simulations, we define a function Δp that characterizes the average pressure difference between ideal Couette rotation and boundary rotation,

$$\Delta p = \frac{\rho r_g^3 \Delta \Omega^2}{\Delta r} \int_{s_1}^{s_2} \int_{s_1}^s (\omega_C^2 - \omega_b^2) s' ds' ds. \quad (3)$$

For the **wide-ring** configuration the zeros of Δp and Φ_z are widely separated, meaning that no circumstance exists where pressure balance and zero net axial flux can be simultaneously satisfied. In contrast, the HTX configuration has zeros of these functions that are nearly

coincident and fall within the operating range in which small fluctuations were observed in Ref. [7]. Other boundary configurations with $q = 1.5$ also have nearly coincident zeros of Φ_z and Δp , in remarkably good agreement with experiments. Note that the requirement of coincident or nearly-coincident zeros represents an effective third constraint. These studies suggest that the requirements of having nearly coincident zeros of Φ_z and Δp for the generation of ideal flows may represent necessary and sufficient conditions. Additional research conducted over a wider range of geometries and shear conditions will provide a stronger test of this hypothesis.

B. Departure of flows from ideal Couette

While the coincident vanishing of Φ_z and Δp define what may be necessary and sufficient conditions for ideal flows to develop, they do not reveal how QK systems should behave under non-optimized conditions. A general model of the fluid response to forcing by the boundaries must account for the fluxes across both axial and radial boundary layers. As there does not exist a theory of Stewartson boundary layers under the conditions of QK rotation at large Reynolds numbers, we cannot rely on results derived from a linear analysis of perturbative differences in rotational speeds [24], especially for experimental conditions where the Stewartson boundary layers are turbulent [7]. Instead, we assume a generalized scaling of the Stewartson boundary layer thickness of the form $\delta_S = \alpha_S r \text{Re}_b^\beta$, taking the exponent of the Reynolds number (β) as a free-parameter to be determined from the observed scalings in Fig. 2. While the numerical factors α_E and α_S are introduced through the definitions of the boundary layer thicknesses, we cannot measure the boundary layers directly, and therefore we must interpret their meaning as a measure of the effectiveness of angular momentum flux.

We begin this analysis by considering the **Ekman** configurations from Fig. 2 where we note that v_θ transitions to solid body rotation at Ω_2 near the outer cylinder, implying that $\Phi_2 \approx 0$. With a jump in azimuthal velocity (a negative Δv) occurring over a Stewartson layer at the inner cylinder, the appropriate form for Φ_1 is

$$\Phi_1 = -\Phi_0 \frac{c_1}{2\alpha_S} \text{Re}_s^\beta \frac{r_1 \Delta v}{\nu}, \quad (4)$$

where $c_1 = (r_1 \Omega_1 / r_2 \Delta \Omega)^\beta$ is a result of converting from a representation of the boundary

layer thickness that depends on the local Re_b to a global Re_s . We approximate these flows with a piecewise function of the form $v_\theta(r_a < r < r_t) = v_C + \Delta v$ and $v_\theta(r_t < r < r_2) = r\Omega_2$, where r_t is the transition radius, similar to the identification of separate flow regions in the recent work of Nordsiek *et al.* [21]. Substituting this rotation profile into Eq. 2 (using $\omega = v_\theta/r\Delta\Omega$) and using Eq. 4 for the radial flux at r_1 , we solve the global balance of angular momentum, $\Phi_1 + 2\Phi_z = 0$, for the dimensionless $\Delta v'_{\text{neg}} = \Delta v/r_g\Delta\Omega$ as a function of Re_s . Noting that Φ_z has two parts given this representation, our solution has three terms and is of the form

$$\Delta v'_{\text{neg}} = \frac{f_1}{\alpha c_1 \frac{L}{2r_2} \text{Re}_s^{\beta-1/2} + f_2}, \quad (5)$$

where $\alpha = \alpha_E/\alpha_S$, and the integral expressions f_1 and f_2 are defined as

$$f_1 = \int_{s_1}^{st} (\omega_b - \omega_C) \omega_b^{1/2} s^3 ds \quad (6)$$

$$f_2 = \int_{s_1}^{st} \omega_b^{1/2} s^2 ds. \quad (7)$$

Equation 5 is a transcendental expression in Δv since the limits of the integrals in f_1 and f_2 are functions of r_t which itself depends on Δv . Equation 5 has only two free parameters: β and $\alpha = \alpha_E/\alpha_S$. Comparison of Eq. 5 with experimental measurements of Δv is presented in Fig. 5 for the $q = 1.8$ and $q = 1.5$ cases, where values of $\beta \approx 0.08$ and $\alpha_E/\alpha_S \approx 15$ provide the best fit to the experimental measurements.

This analysis can be extended to the case of the **Split** configuration with positive Δv by accounting for the different boundary conditions and a slightly more complex flow structure. The most important feature of the positive Δv cases is that there is a nearly linear decrease in Δv across the gap, where Δv at r_2 is defined to be equal to $\epsilon\Delta v$. In the $q = 1.8$ cases Δv decreases by about 60% across the gap ($\epsilon = 0.4$), and by 80% for $q = 1.5$ ($\epsilon = 0.2$), nearly independent of Reynolds number. The radial flux at r_2 in terms of the ϵ reduced Δv is

$$\Phi_2 = \Phi_0 \frac{c_2}{2\alpha_S} \text{Re}_s^\beta \frac{r_2\epsilon\Delta v}{\nu}, \quad (8)$$

where $c_2 = (r_2\Omega_2/r_1\Delta\Omega)^\beta$. The solution for positive, normalized Δv is

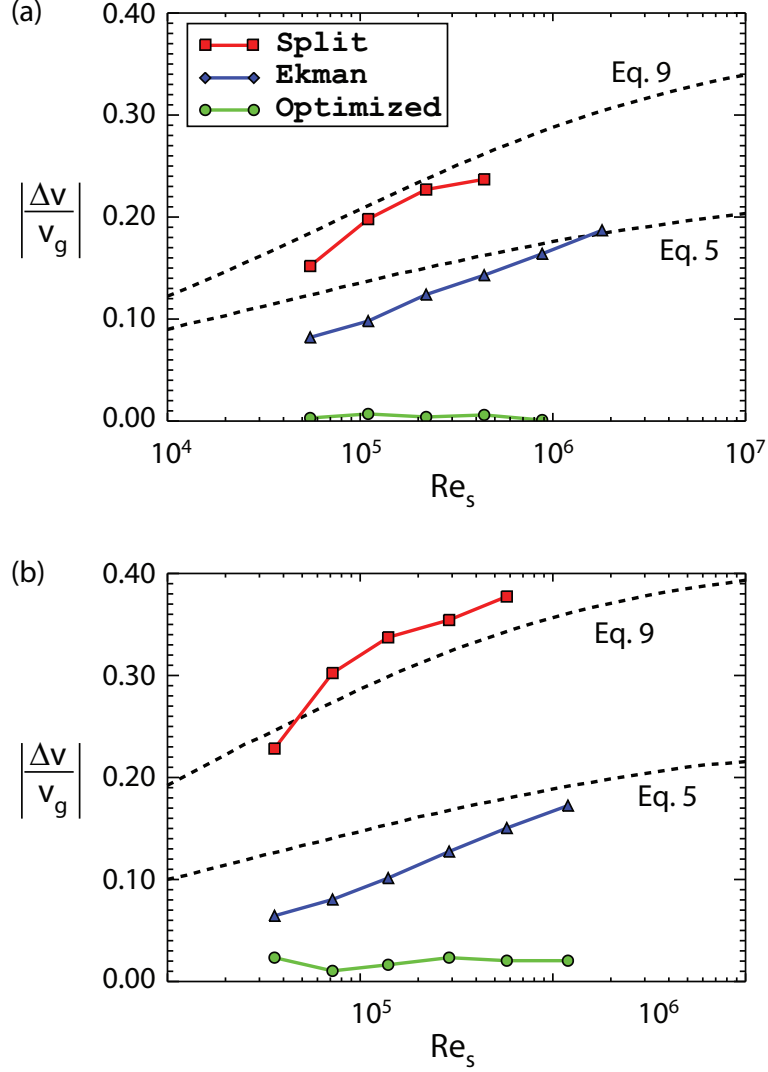


FIG. 5. (color online) Scaling of the velocity differential Δv for the three groups of boundary conditions from Fig. 2 for (a) $q = 1.8$ and (b) $q = 1.5$. The dashed lines in the figure are the solutions to Eqs. 5 and 9 with $\beta = 0.08$ and $\alpha_E/\alpha_S = 15$.

$$\Delta v'_{pos} = \frac{f_3}{\epsilon \alpha c_2 \frac{L}{2r_1} Re_s^{\beta-1/2} + f_4}, \quad (9)$$

where, similar to Eq. 5, we have

$$f_3 = \int_{s_t}^{s_2} (\omega_b - \omega_C) \omega_b^{1/2} s^3 ds \quad (10)$$

$$f_4 = \int_{s_t}^{s_2} \left[\frac{s_2 - \epsilon s_t - (1 - \epsilon)s}{s_2 - s_t} \right] \omega_b^{1/2} s^2 ds. \quad (11)$$

For the **Split** cases, the term s_t defines the transition point from increasing to decreasing Δv , and the terms in square brackets in Eq.11 derive from the variation of Δv with radius (note that if Δv were constant across the gap then $\epsilon = 1$ and the term in brackets reduces to unity, recovering Eq. 7). Equation 9 is compared against the measured $\Delta v'$ in Fig. 5 and is also found also to be in good agreement with experiment when using the same values of α_E/α_S and β derived from the analysis of the **Ekman** cases.

The success of this model in reproducing the general features of the departures from ideal Couette is remarkable given that it represents a simple accounting of the angular momentum fluxes across the boundaries, ignoring completely the complex internal dynamics of these flows, especially at large Reynolds number where a substantial fraction of the volume exhibits turbulent fluctuations [7]. What disagreement exists between experiment and theory should not overshadow the success of this model in reproducing the general trend of the velocity deviations, the relative amplitude of the positive and negative Δv cases, and the change in the amplitude of the positive Δv cases between $q = 1.8$ and $q = 1.5$. While the model presented here uses a single set of parameters for both values of q , better fits to the data can be found if we let these parameters depend on q . It is also possible the these parameters have some dependence on geometry and themselves have a dependence on Reynolds number that is not captured by the power-law scaling used here.

Studies of the measured fluctuation levels arising from the Stewartson boundary layers in Ref. [7] found that the transition to turbulent Stewartson boundary layers was consistent with the Taylor model of low Reynolds number centrifugal instability. So while cannot offer a precise explanation for why β should take a value close to 0.1, we reiterate that the inferred scaling applies to the angular momentum flux which is a combination of variations in the boundary layer thickness and an effective viscosity within these layers that is modified by turbulent fluctuations. It is beyond the scope and ability of these experiments to identify the separate scalings of the turbulent viscosity and the thickness of the Stewartson boundary layers, though perhaps future experiments will be able to provide greater insight into this problem.

IV. CONCLUSIONS

We conclude with an outlook to future physical and numerical experiments. The ratio of Φ_z and Φ_C explored earlier can be recast as a constraint on the aspect ratio $L/\Delta r$ as a function of the Reynolds number. The relative contribution of Φ_z can be made arbitrarily small by increasing the axial size of the system, so that to make $\Phi_z/\Phi_C \approx 10^{-2}$ for an Ekman configuration, for example, one would need an aspect ratio of order 100 at a Reynolds number of 10^6 . Outside of using very large aspect ratios, one can employ mechanical advantages as we have done in HTX, such as extensions of the inner and outer cylinder or independent rings. Despite the desire to simplify the mechanical design of such modified TC devices, further analysis shows that the only way to achieve simultaneous zeros in Φ_z and Δp is through a design with at least one independent ring. Greater insight into the balance of forces in quasi-Keplerian flows could be explored in future experiments in modified Taylor Couette devices like HTX. In particular, further exploration of the Reynolds number dependence on these deviations, the dependence of the model parameters on q , and the structure of the Ekman cells would tell us much more about the influence of the boundaries on global behavior.

We have shown that nearly ideal flows exhibit profile shape invariance under scaling of the Reynolds number, an effect we interpret through the dual conditions of vanishing axial angular momentum flux and vanishing pressure differential that are nearly simultaneously satisfied, offering predictive capability for selecting optimized boundary conditions and in experimental design. The strongest piece of evidence in support of this model is the prediction of self-similarity of the profiles with respect to scaling of the Reynolds number only for cases in which the axial flux of angular momentum and the pressure differential vanish nearly coincidentally, a prediction in excellent agreement with the observations presented in Fig. 2. It should be reiterated that while the experiments for `Optimized` flows show very small departures from ideal Couette, and whose interpretation is congruent with the coincident zeros in Δp and Φ_z , this does not strictly prove that these criteria represent true sufficient conditions. An interesting problem for future studies would be to measure how the departures from ideal Couette depend on the “distance” between these zeros.

It is interesting to note that in all cases presented here the local axial fluxes of angular momentum may be quite large given the substantial difference in speed between the bulk fluid

and the axial boundaries, and that it is only on summation over the axial boundaries that zero net axial flux is realized for the `Optimized` cases. Recalling that multiple experiments [7, 19, 20] and simulations [25, 27] have observed a nearly uniform axial structure through the bulk of the fluid volume, the existence of the large axial fluxes naturally raises the question of what allows the bulk flows to depart from the solid body rotation forced by the boundaries? Intuition based on the Taylor-Proudman theorem for Rayleigh-stable flows, that is $dv_\theta/dz \approx 0$, would suggest that the bulk should tend to follow the boundary. However, it should be recalled that the Ekman boundary layers do not need to satisfy the Taylor-Proudman theorem because the axial gradient of v_θ is balanced with a viscous diffusion of vorticity over the scale of the boundary layer thickness. Thus, the nearly uniform axial structure suggests that the large fluxes of angular momentum that must be present due to the existence of the the Ekman boundary layers are redistributed locally, perhaps by small Ekman cells that do not extend far into the bulk of the fluid or even in the boundary layers themselves. As has been shown in prior studies, the free-shear layer that develops at the interface between the differentially rotating rings on the axial boundaries is expected to be centrifugally unstable and may help to enhance the redistribution of angular momentum locally [13].

Another problem for future experiments, both physical and numerical, will be to explore in greater detail how the very large, local fluxes of angular momentum are redistributed near the axial boundaries with only minor effect on the bulk flow in the `Optimized` configurations. Non-optimized boundaries, like the `Split` and `Ekman` configurations, show progressive departure from the ideal Couette flow as the Reynolds number is increased, in agreement with the expectations of a dominant axial flux of angular momentum. A good test for numerical experiments will be to accurately model the global behavior of the mean flows in TC experiments by properly accounting for the angular momentum fluxes from the boundaries. We believe that the boundary layer scalings presented here may enable simulations to bootstrap to larger effective Reynolds numbers by using specified boundary flux models, thus bypassing the need for very fine grids to resolve the boundary layer structure directly. With the combination of recent simulations of QK flows that can attain Reynolds numbers of the order of 10^5 [14, 28], though with axially-periodic boundary conditions, a specified-flux boundary model may allow simulations to reach something resembling experimental conditions of large Reynolds number TC flows.

ACKNOWLEDGEMENT

We would like to thank J. Goodman for sharing his thoughts on angular momentum transport and boundary layers in our studies, and E. Schartman, E. Gilson, and P. Sloboda in helping to keep the experiments running smoothly. This work was supported by the U.S. Department of Energy, Fusion Energy Sciences under contract DE-AC02-09CH11466.

-
- [1] A. Adams, P. M. Chesler and H. Liu, *Phys. Rev. Lett.* **112**, 151602 (2014).
 - [2] F. Carrasco, L. Lehner, R. C. Myers, O. Reula and A. Singh, *Phys. Rev. D* **86**, 126006 (2012).
 - [3] J. E. Rice J. W. Hughes, P. H. Diamond, Y. Kosuga, Y. A. Podpaly, M. Reinke, M. J. Greenwald, Ö. D. Gürçan, T. S. Hahm, A. E. Hubbard, E. S. Marmor, C. J. McDevitt and D. G. Whyte, *Phys. Rev. Lett.* **106**, 215001 (2011).
 - [4] O. D. Gürçan, P. H. Diamond, C. J. McDevitt and T. S. Hahm, *Phys. Plasmas* **17**, 032509 (2010).
 - [5] H. Ji, M. Burin, E. Schartman and J. Goodman, *Nature* **444**, 343 (2006).
 - [6] E. Schartman, H. Ji, M. Burin and J. Goodman, *Astron. Astrophys.* **543**, A94 (2012).
 - [7] E. M. Edlund and H. Ji, *Phys. Rev. E* **89**, 021004 (2014).
 - [8] M. S. Paoletti and D. P. Lathrop, *Phys. Rev. Lett.* **106**, 024501 (2011).
 - [9] M. Seilmayer, V. Galindo, G. Gerbeth, T. Gundrum, F. Stefani, M. Gellert, G. Rüdiger, M. Schultz and R. Hollerbach, *Phys. Rev. Lett.* **113**, 024505 (2014).
 - [10] F. Stefani, T. Gundrum, G. Gerbeth, G. Rüdiger, M. Schultz, J. Szklarski and R. Hollerbach, *Phys. Rev. Lett.* **97**, 184502 (2006).
 - [11] D. R. Sisan, N. Mujica, W. A. Tillotson, Y. Huang, W. Dorland, A. B. Hassam, T. M. Antonsen and D. P. Lathrop, *Phys. Rev. Lett.* **93**, 114502 (2004).
 - [12] A. H. Roach, E. J. Spence, C. Gissinger, E. M. Edlund, P. Sloboda, J. Goodman and H. Ji, *Phys. Rev. Lett.* **108**, 154502 (2012).
 - [13] E. J. Spence, A. H. Roach, E. M. Edlund, P. Sloboda and H. Ji, *Phys. Plasmas* **19**, 056502 (2012).
 - [14] R. Ostillo-Monico, R. Verzicco, S. Grossmann and D. Lohse, *J. Fluid Mech.* **748**, R3 (2014).
 - [15] S. Maretzke, B. Hof and M. Avila, *J. Fluid Mech.* **742**, 254 (2014).

- [16] D. S. Zimmerman, S. Andrés Triana and D. P. Lathrop, *Phys. Fluids* **23**, 065104 (2011).
- [17] S. G. Huisman, R. C. A. van der Veen, C. Sun and D. Lohse, *Nature Communications* **5**, 3820 (2014).
- [18] G. Lesur and P.-Y. Longaretti, *Astron. Astrophys.* **444**, 25 (2005).
- [19] M. Burin, H. Ji, E. Schartman, R. Cutler, P. Heitzenroeder, W. Liu, L. Morris and S. Raftopolous, *Experiments in Fluids* **40**, 962 (2006).
- [20] E. Schartman, H. Ji and M. Burin, *Rev. Sci. Instrum.* **80**, 024501 (2009).
- [21] F. Nordsiek, S. G. Huisman, R. C. A. van der Veen, C. Sun, D. Lohse and D. P. Lathrop, *J. Fluid Mech.* **774**, 342 (2015).
- [22] D. A. Bennetts and L. M. Hocking, *Proc. R. Soc. A.* **333**, 469 (1973).
- [23] D. J. Baker, *J. Fluid Mech.* **29**, 165 (1967).
- [24] K. Stewartson, *J. Fluid Mech.* **3**, 17 (1957).
- [25] A. V. Obabko, F. Cattaneo and P. F. Fischer, *Phys. Scr.* **T132**, 014029 (2008).
- [26] O. Czarny, E. Serre, P. Bontoux and R. Leuptow, *Phys. Fluids* **15**, 467 (2003).
- [27] M. Avila, *Phys. Rev. Lett.* **108**, 124501 (2012).
- [28] L. Shi, M. Rampp, B. Hof and M. Avila, *Computers & Fluids* **106**, 1 (2015).